Since January 2020 Elsevier has created a COVID-19 resource centre with free information in English and Mandarin on the novel coronavirus COVID-19. The COVID-19 resource centre is hosted on Elsevier Connect, the company's public news and information website.

Virology 511 (2017) 9–18

Contents lists available at ScienceDirect

Virology

journal homepage: www.elsevier.com/locate/yviro

Lipidation increases antiviral activities of coronavirus fusion-inhibiting peptides

Jung-Eun Park[1], Tom Gallagher[*]

Department of Microbiology and Immunology, Loyola University Chicago, Maywood, IL 60153, USA

ARTICLE INFO

Keywords:
Coronavirus
Virus entry
Virus-cell fusion
Proteolytic activation
Antiviral agents
Fusion-inhibiting peptide
Lipopeptide

ABSTRACT

Coronaviruses (CoVs) can cause life-threatening respiratory diseases. Their infectious entry requires viral spike (S) proteins, which attach to cell receptors, undergo proteolytic cleavage, and then refold in a process that catalyzes virus-cell membrane fusion. Fusion-inhibiting peptides bind to S proteins, interfere with refolding, and prevent infection. Here we conjugated fusion-inhibiting peptides to various lipids, expecting this to secure peptides onto cell membranes and thereby increase antiviral potencies. Cholesterol or palmitate adducts increased antiviral potencies up to 1000-fold. Antiviral effects were evident after S proteolytic cleavage, implying that lipid conjugates affixed the peptides at sites of protease-triggered fusion activation. Unlike lipid-free peptides, the lipopeptides suppressed CoV S protein-directed virus entry taking place within endosomes. Cell imaging revealed intracellular peptide aggregates, consistent with their endocytosis into compartments where CoV entry takes place. These findings suggest that lipidations localize antiviral peptides to protease-rich sites of CoV fusion, thereby protecting cells from diverse CoVs.

1. Introduction

Coronaviruses (CoVs) are enveloped RNA viruses that can infect the respiratory and enteric tracts of birds and mammals. Their virulence to host animals varies from asymptotic to life-threatening, depending on the infecting virus type and on host susceptibility determinants (Channappanavar and Perlman, 2017; de Wit et al., 2016; Graham et al., 2013; Weiss and Navas-Martin, 2005; Weiss and Leibowitz, 2011). The CoVs are known for their zoonotic transmissibility to humans, as revealed by the sudden emergence of severe acute respiratory syndrome (SARS) in 2002 (Lau et al., 2005; Li et al., 2005) and Middle East respiratory syndrome (MERS) in 2012 (Annan et al., 2013; Anthony et al., 2017; Memish et al., 2014). Antiviral agents that can limit MERS-CoV and newly-emerging CoV infections will reduce the disease burdens and quell fears about future epidemics originating from zoonotic CoVs.

CoV spike (S) proteins emanate from infecting virus particles, where they adhere to cellular receptors on target cells and then catalyze viral envelope-cellular membrane fusion (Belouzard et al., 2012; Simmons et al., 2013). Atomic-resolution structures are known for five CoV S proteins (Gui et al., 2017; Kirchdoerfer et al., 2016; Walls et al., 2016a, 2016b; Yuan et al., 2017). They are large ~ 500 kDa homotrimers, with each monomer comprising several domains. The Receptor-Binding Domains (RBDs) are distant from virion envelopes, while the Fusion-catalyzing Domains (FDs) are virus-proximal and buried underneath the canopy of RBDs. Similar to the fusion-catalyzing proteins of all enveloped viruses, the CoV S proteins are produced in inactive “pre-fusion” states, becoming activated (i.e., capable of catalyzing membrane fusion) only after undergoing structural transitions during cell entry. Environmental factors controlling S protein activation are encountered during cell entry and include cellular receptors, which bind to particular S protein conformations (Gui et al., 2017) and may promote “fusion-ready” states (Matsuyama and Taguchi, 2009; Park et al., 2016; Zelus et al., 2003). The second factors are cellular proteases, which cleave S proteins and permit further structural changes (Belouzard et al., 2009; Matsuyama et al., 2006; Simmons et al., 2005). While many details of the structural dynamics remain unknown, current speculations are that receptor binding and proteolysis exposes FDs and allows their hydrophobic “fusion peptide” portions to embed into target cell membranes (Yuan et al., 2017). The result is a putative alpha-helical “extended fusion intermediate” linking viruses to host cells, which, after an undefined time period, collapses in concert with the coalescence of viral and cell membranes. The post-fusion FDs are highly-stable, permanently inactive, collapsed antiparallel helical bundles (Bosch et al., 2003; Gao et al., 2013; Lu et al., 2014).

* Corresponding author.
E-mail address: tgallag@luc.edu (T. Gallagher).
[1] Research Institute of Veterinary Medicine, College of Veterinary Medicine, Chungnam National University, 99 Daehak-ro, Yuseong-gu, Daejeon 34134, Republic of Korea.

http://dx.doi.org/10.1016/j.virol.2017.07.033
Received 17 May 2017; Received in revised form 25 July 2017; Accepted 27 July 2017
Available online 10 August 2017
0042-6822/

Peptides highly similar or identical to a membrane-proximal portion of S protein FDs can block this fusion process and thereby prevent CoV infections. These ~ 30 amino acid peptides, designated as Heptad Repeat 2 (HR2) peptides, bind to an FD region called HR1, forming antiparallel helical bundles. HR2 peptides only bind to fusion intermediates, not to pre- and post- fusion S proteins, and interfere with refolding into post-fusion FDs, (Bosch et al., 2004; McReynolds et al., 2008; Xu et al., 2004a, 2004b). Many enveloped viruses undergoing similar fusion catalysis, including human immunodeficiency virus (Jiang et al., 1993; Wild et al., 1994), paramyxoviruses (Lambert et al., 1996; Rapaport et al., 1995; Young et al., 1997), and flaviviruses (Hrobowski et al., 2005), are subject to analogous suppression by fusion-inhibitory peptides. However, CoV HR2 peptides inhibit virus infection in the micromolar range (Bosch et al., 2004; Gao et al., 2013; Liu et al., 2013; Lu et al., 2014; Xu et al., 2004c), and are therefore only weakly antiviral, at least in comparison with HIV-1 gp41 HR2 peptides, which prevent HIV-cell entry when present in low nanomolar concentrations (Wild et al., 1994).

One explanation for these modest antiviral activities is that the CoV FD intermediates are formed at subcellular locations that are not accessible to the HR2 peptides. These inaccessible locations may be within membrane microdomains (Choi et al., 2005; Earnest et al., 2015; Lu et al., 2008; Nomura et al., 2004; Thorp and Gallagher, 2004) or within endosomes (Bosch et al., 2008a; Kawase et al., 2009; Qiu et al., 2006; Shah et al., 2010; Simmons et al., 2005). These are protease-enriched locations that one might expect to facilitate S protein activation. Exogenously-added HR2 peptides may not accumulate in these protease-enriched subcellular environments, with the result being somewhat modest antiviral effects. Thus we speculated that the HR2 peptides might have increased antiviral potencies if they were concentrated into the locations where S-directed fusions take place. The present study provides evidence that CoV S proteins must be proteolyzed to form the fusion intermediates that are targeted by HR2 peptides, and evaluates adducts that might concentrate HR2 peptides into protease-rich regions. The findings indicate that lipid adducts greatly increase HR2 peptide antiviral activities, and suggest that the lipidated HR2 peptides accumulate at locations where incoming viruses undergo transitions into fusion intermediates.

2. Results

2.1. Antiviral activities of lipid-conjugated HR2 peptides

The HR2 peptides used in this study were designed by Jiang and colleagues (Lu et al., 2014), and were engineered to specifically inhibit MERS-CoV (Channappanavar et al., 2015; Gao et al., 2013; Lu et al., 2014). This study evaluated lipophilic derivatives of these "MERS HR2P-M2″ peptides. The custom-synthesized peptides, prepared by American Peptide Company, Sunnyvale, CA, all included a C-terminal glycine-serine-glycine (GSG) linker, then four ethylene glycols (dPEG4), and then a particular lipid moiety (Fig. 1A). The lipids were selected on the basis of their incorporation into different membrane microdomains; cholesterol and palmitate were chosen because they embed into lipid rafts (Schumann et al., 2011) and tocopherol was selected for its differential inclusion into polyunsaturated fatty acid (PUFA) enriched non-raft like domains (Atkinson et al., 2010; Raederstorff et al., 2015). CoV receptors and proteases are transmembrane-anchored and enriched in lipid raft-like microdomains (Andre et al., 2006; Earnest et al., 2015; Le Naour et al., 2006; Rana et al., 2011), making it likely that S protein intermediates are formed in these restricted membrane locations. Therefore, HR2 peptides might be extraordinarily antiviral if they were C-terminally embedded in or very near these microdomains, as might be the case for cholesterol and palmitate, but perhaps not for tocopherol-conjugated peptides.

We asked whether the lipid-conjugated MERS HR2 peptides can inhibit CoV infections. The first virus to be evaluated was *Mouse Hepatitis Virus* (MHV), a beta-CoV with moderate homology to MERS-CoV (van Boheemen et al., 2012), and having sites to which HR2 binds (i.e., "HR1 target" sites) that are 56% similar to those on MERS-CoV S proteins (Fig. 1B). Human HEK293 cells expressing the MHV receptor carcinoembryonic antigen-related cell adhesion molecule 1a (CEACAM1a) (Williams et al., 1991) were incubated for one hour with graded doses of the lipopeptides, and then challenged with recombinant MHV (strain A59) encoding a firefly luciferase (Fluc) reporter (Shulla and Gallagher, 2009). Infections, as measured by the Fluc accumulations, were potently reduced > 100- and > 1000-fold by 1 μM concentrations of cholesterol- and palmitate- tagged HR2 peptides, respectively (Fig. 2A). By contrast, infections were reduced only 10-fold and ~ 2-fold by tocopherol- and dPEG4-tagged HR2 peptides (Fig. 2A). The IC90 values for cholesterol- and palmitate-HR2 peptides were ~ 100 nM. These findings indicated that lipidations potently increased HR2 antiviral activities, and extended their antiviral activities to a CoV that has only moderate identity with MERS-CoV (see Fig. 1B).

To focus more specifically on virus-cell entry stages, we next asked whether the lipopeptides arrest S protein-driven cell entry. This was accomplished using human immunodeficiency virus (HIV) based pseudo-particles (pps) that contain CoV S proteins. The CoV S proteins transduce HIV genome-encoded Fluc genes, thus Fluc accumulations in target cells reflect S-directed virus entry. We constructed pps displaying MHV (strain A59) S proteins, and then transduced the HEK293-MHV receptor-bearing cells. Subsequently, extents of transduction were measured by luciferase accumulations. The results paralleled those observed in evaluations of authentic MHV infection (compare Figs. 2A and 2B). These findings demonstrated that the HR2 antiviral effects operate entirely at the cell entry stage, and they also engendered confidence that the pp transductions reflect authentic CoV-cell entry events.

Using this validated pp transduction approach, we determined whether HR2 peptides blocked several different S-directed virus entry processes. We constructed pps with control vesicular stomatitis virus (VSV) glycoprotein (G) proteins, or with MERS, SARS, or human CoV strain 229E S proteins. HEK293 target cells for these pps were then established by transfecting the necessary cellular receptors; human dipeptidyl peptidase-4 (DPP4) for MERS pps (Raj et al., 2013), human Angiotensin-converting enzyme 2 (ACE2) for SARS pps (Li et al., 2003), and human aminopeptidase N (APN) for 229E pps (Yeager et al., 1992). These cells were then transduced in the presence of graded HR2 doses. Under these conditions, the VSV pp transductions were unaffected by any HR2 (Fig. 2C). SARS and 229E pp transductions were significantly reduced only by the palmitate-tagged HR2 peptides (Figs. 2D and 2E; compare zero HR2 to 1 μM palm). However, MERS pp transductions were reduced in a pattern similar to that of MHV, with cholesterol- and palmitate- tagged HR2 peptides having IC50s in the 100 nM range, and the dPEG4- and tocopherol- tagged HR2 peptides having less convincing antiviral effects (Fig. 2F). These results indicate that the covalently-attached lipids cholesterol and palmitate significantly increase HR2 antiviral potencies, with palmitate also broadening their antiviral activity spectrums, even to the 229E spikes that have divergent HR1 target sites (see Figs. 1B and 2E).

2.2. Relationships between HR2 peptide antiviral activities and CoV-activating proteases

The exceedingly weak antiviral activities of lipid-free dPEG4 peptides appeared inconsistent with a nearly identical HR2P-M2 being able to protect mice from MERS-CoV infection in mouse lungs (Channappanavar et al., 2015). Therefore we considered whether the HR2 peptides, particularly the lipid-free HR2, might be evidently antiviral in other cell types, and if so, whether particular cellular factors correlate with antiviral effect. Two cell types were selected; Calu3, a human lung-derived cell line (Shen et al., 1994) and Vero81, a standard line for propagating human CoVs. Here we found that the

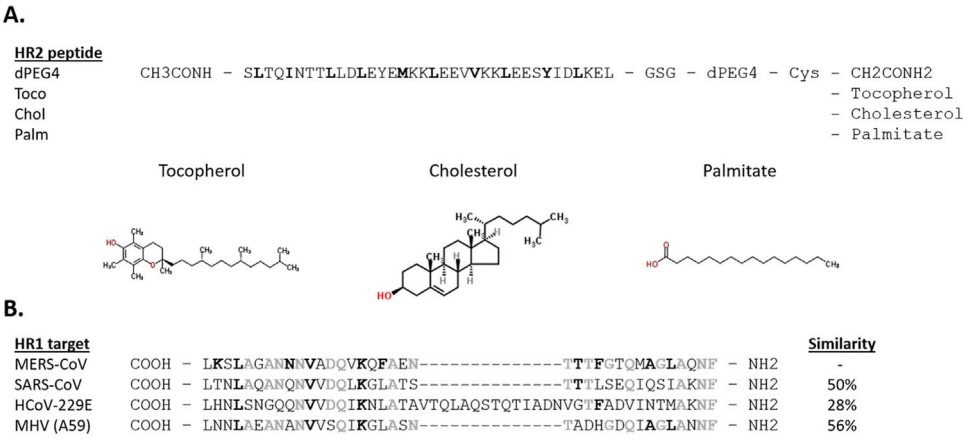

Fig. 1. Design of HR2 peptides and sequence similarities of the CoV HR1 regions. (A) The sequences of the designed HR2 peptides and the structures of lipids that are attached to the HR2 peptide are shown. The residues that interact with HR1 target are highlighted in bold font. (B) Sequence similarities between the HR1 targets of MERS-CoV, SARS-CoV, HCoV-229E, and MHV strain A59 are shown. The similarity scores were calculated using Align software (http://www.uniprot.org/align/) and indicate the similarity of each HR1 target to that of MERS-CoV. The residues that interact with HR2 peptides are highlighted in bold font and residues located at non-interacting regions are shaded in gray.

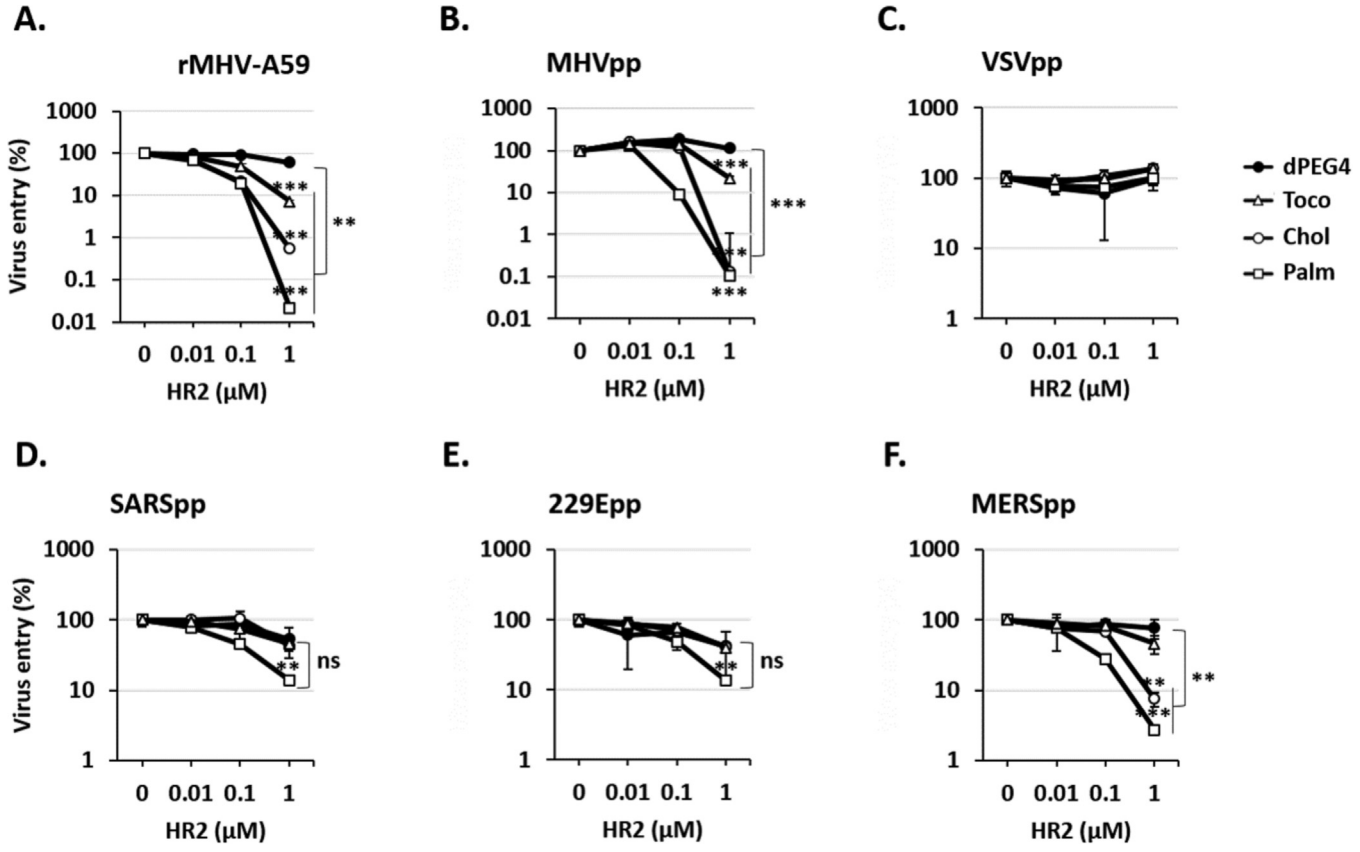

Fig. 2. Inhibition of CoV entry by lipid-conjugated HR2 peptides. (A) HEK293 cells expressing mCEACAM1a were infected with recombinant MHV strain A59 in the presence of increasing concentrations of indicated HR2 peptides. Virus entry was quantified by measuring luciferase levels at 5 h post-infection. (B-F) HEK293 cells expressing appropriate receptors were transduced with MHV (B), VSV (C), SARS (D), 229E (E), and MERS (F) pps in the presence of increasing concentrations of the indicated HR2 peptides. Virus entry was quantified by measuring luciferase levels at 48 h post-transduction. Error bars present SD from the mean (n = 3). Statistical significance was assessed by student's *t*-test. **, $P < 0.01$; ***, $P < 0.001$; ns, not significant compared to no HR2 peptide condition. Brackets at right indicate significance of differences between dPEG4 (non-lipidated) and lipid-conjugated peptide antiviral activities.

lipid-free (dPEG4) HR2 peptides showed significant antiviral effects in the Calu3, but not in the Vero81 cell lines (Fig. 3A). This finding prompted attempts to identify the cell type-specific factors that account for the differential HR2 antiviral potencies. For MERS-CoV, the principal cell entry factors include the virus receptor DPP4, and the fusion-triggering proteases *T*rans-*M*embrane *PR*otease (TMPR) *S*erine *S*ubtype *2* (TMPRSS2) (Gierer et al., 2013; Shirato et al., 2013), furin (Millet and Whittaker, 2014), and cathepsin L (Qian et al., 2013). Using quantitative RT-PCR, we measured relative transcript levels of these factors in the two cell lines. Of the four factors, TMPRSS2 was clearly the most variable, being undetectable in the Vero81 cell line (Fig. 3B).

To further address possible correlations between TMPRSS2-like proteases and HR2 antiviral activity, we evaluated MERSpp entry in the presence of camostat, a specific TMPR inhibitor (Shirato et al., 2013). In the two tested cell lines, the antiviral activities of camostat

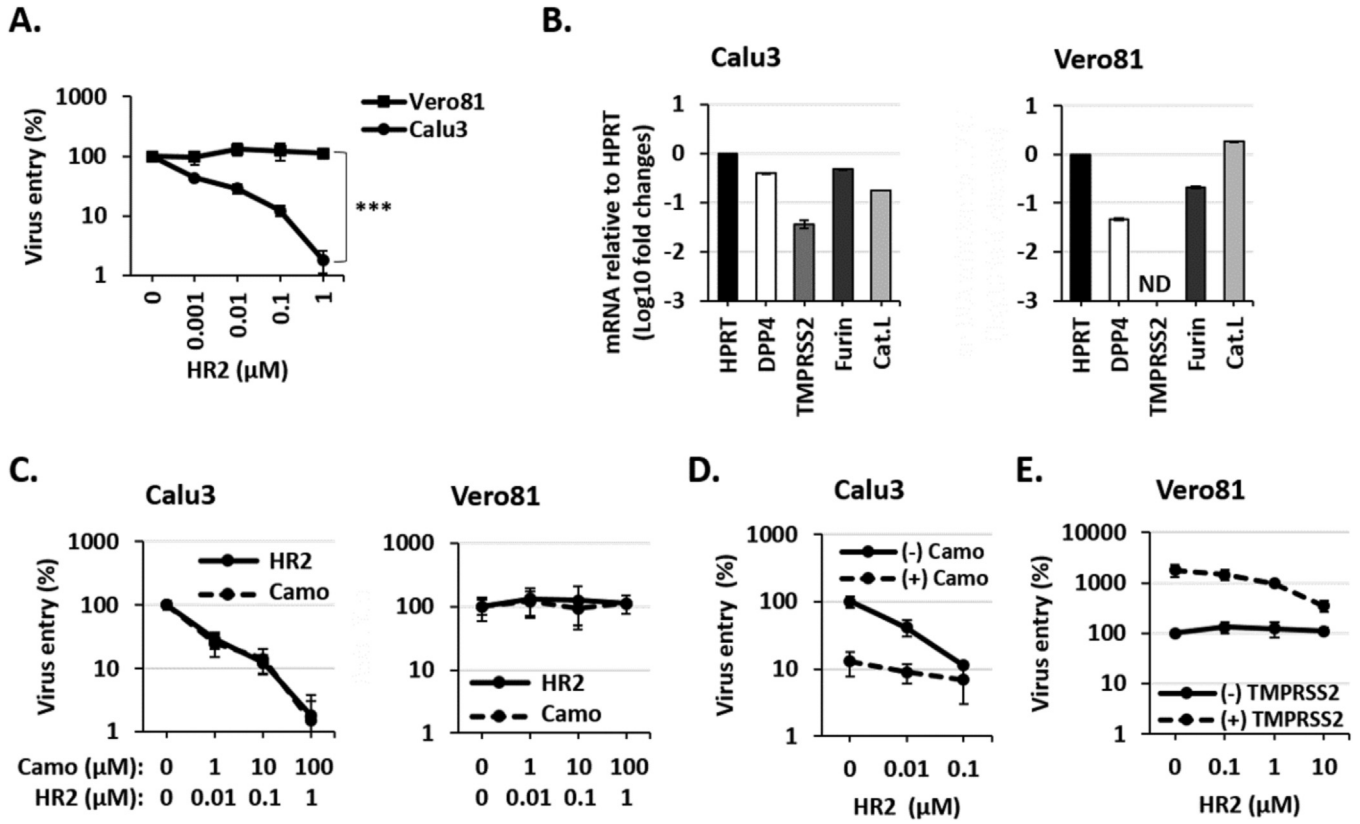

Fig. 3. Effects of cell-surface proteases on HR2 peptide antiviral activities. (A) Calu3 and Vero81 cells were incubated with MERS pps in the presence of increasing concentrations of HR2 peptides. (B) Total cellular RNA was isolated from Calu3and Vero81 cells, and evaluated for the expression of DPP4, TMPRSS2, furin, cathepsin L (Cat. L) and hypoxanthine-guanine phosphoribosyltransferase (HPRT) transcripts by reverse transcription – quantitative PCR. Expression levels were plotted relative to HPRT expression levels. ND = Not Detected. (C) Calu3 and Vero81 cells were transduced with MERS pps in the presence of increasing concentrations of HR2 peptide or camostat (Camo). Camo was present from 1 h pre-transduction and HR2 was present at the time of MERS pp inoculation. (D) Calu3 cells were incubated with or without 10 μM camostat (Camo) for 1 h, then transduced with MERS pps in the presence of increasing concentrations of HR2 peptide. (E) Vero81 cells were transfected with either TMPRSS2 or vector control plasmids. At 2 d post-transfection, cells were transduced with MERS pps in the presence of increasing concentrations of HR2 peptide. For (A), (C), (D) and (E), unbound MERS pps and entry inhibitors were removed at 1 h post-transduction. Virus entry was quantified by measuring luciferase levels at 48 h post-transduction and data were normalized to control conditions lacking inhibitors. Error bars present SD from the mean (n = 3). Statistical significance was assessed by student's *t*-test. ***, P < 0.001.

and HR2 were roughly similar to each other. Both agents were potently antiviral in Calu3 cells, yet completely inert in Vero81 cells (Fig. 3C), suggesting strong correlations between TMPR activities and unlipidated HR2 antiviral activities. We further investigated these relationships by assessing HR2 antiviral activities at different TMPR levels. To decrease TMPRs in Calu3 cells, camostat was added at a dose that reduces MERS pp entry to ~10% of normal (Figs. 3C and 3D). MERS pp transductions into Calu3 cells having this diminished TMPR activity were only modestly suppressed about 2-fold by HR2 peptides, while in the control conditions of full TMPR activity, the HR2 peptides suppressed pp entry ~ 10-fold (Fig. 3D). To increase TMPRs in Vero81 cells, TMPRSS2 plasmids were transfected, and then the TMPRSS2-positive cells were inoculated with MERS pps and HR2 peptides. MERS pp transductions into Vero cells having ectopic TMPRSS2 were suppressed about 6-fold by HR2 peptides, while transductions into control-transfected Vero cells were unaffected by HR2 (Fig. 3E). These results support the hypothesis that S protein cleavages are prerequisites to the S protein conformational changes that generate HR2 peptide-binding sites. The TMPRs mediate this cleavage at cell surfaces, thereby creating binding sites for extracellular unlipidated HR2 peptides.

2.3. Inhibition of endosome-localized CoV entry by lipid-conjugated HR2 peptides

In Vero81 cells, MERS pps traffic to endosomes without undergoing fusion-triggering proteolytic cleavages, and then they become fusion-activated by endosomal cysteine proteases (Shirato et al., 2013). Several other CoVs require a similar endocytosis prior to cytosolic entry (Qiu et al., 2006; Simmons et al., 2005). We asked whether MERS pp entry through this endosomal route is suppressed by any of the HR2 lipopeptides. The cholesterol- and palmitate- tagged HR2 peptides reduced MERS pp entry into the TMPRSS2-null Vero81 cells (Fig. 4D), and also suppressed MERS pp entry into several other cell types that are known to allow CoV entry through endosomes (Fig. 4A–C). Thus it appeared that the lipid adducts brought HR2 peptides into endosomes, where they then bound and inactivated MERS S proteins that had undergone cleavage by endosomal cathepsins.

We further validated this contention by determining whether lipid-tagged HR2 peptides specifically block a CoV pp that was engineered to be highly dependent on endocytosis and cleavage-triggering by endosomal cysteine proteases. We constructed a CoV pp that requires endosomal proteases by ablating TMPR-specific S proteolytic substrate sites, leaving only the cathepsin sites available for cleavage-activation. A TMPR and furin substrate site on MERS S, the “S2-prime” cleavage site (Millet and Whittaker, 2014), was eliminated by mutation from $R_{884}SAR_{887}$ to $S_{884}SYG_{887}$. These “S2′ mut” S proteins were compared with wild-type (WT) S protein-directed pp entry into Caco2 cells. WT MERS pp entry was modestly suppressed by camostat (a TMPR inhibitor), E64d (a cysteine protease inhibitor) and bafilomycin A1 (BafA1, an endosome acidification inhibitor) (Fig. 5A, black bars). These findings that any single inhibitor cannot dramatically reduce transduction were indicative of redundant virus entry pathways – the WT S proteins can direct Caco2-cell entry by either the TMPR / furin -

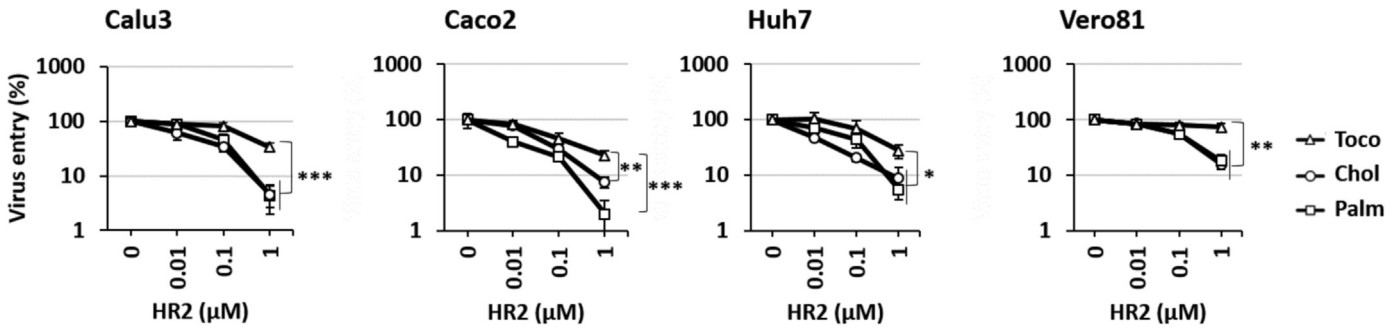

Fig. 4. Inhibition of MERS pp entry by lipid-conjugated HR2 peptides. Calu3 (A), Caco2 (B), Huh7 (C), and Vero81 (D) cells were transduced with MERS pps in the presence of increasing concentrations of indicated lipid-conjugated HR2 peptides. After 1 h, unbound MERS pps and HR2 peptides were removed. Virus entry was quantified by measuring luciferase levels at 48 h post-transduction and normalized to entry levels in the absence of HR2 peptides. Error bars present SD from the mean (n = 3). Statistical significance was assessed by student's *t*-test. *, $P < 0.05$; **, $P < 0.01$; ***, $P < 0.001$.

dependent cell-surface route or the cysteine protease-dependent endosomal route. By contrast, the mutant MERS pps were not suppressed at all by camostat, and were potently blocked by E64d and BafA1 (Fig. 5A, gray bars). These findings indicated that the S2′ mut proteins require a late endosomal entry process.

With the endosome-requiring viruses in hand, we assessed peptide antiviral activities. The lipid-free dPEG4 peptide inhibited WT MERS pps by 2-fold at 1 μM concentration, but did not block late-entering S2′ mut pps (Fig. 5B), consistent with "free" extracellular HR2 accessing only those viruses that activate fusion at cell surfaces. Tocopherol tagged peptides reduced WT and mutant MERS pps equally, but with only modest potency (Fig. 5C). In contrast, cholesterol- and palmitate-tagged HR2 peptides potently and similarly inhibited both the WT and mutant MERS transductions (Fig. 5D and E).

To determine whether the lipid tags do indeed bring the HR2 peptide into endosomes, lipid-free and cholesterol-containing peptides were biotinylated and then incubated with CoV-susceptible cells. Following cell fixation, fluorescent streptavidin was then applied and immunofluorescence microscopy was used to detect cell-associated peptides. By these methods, lipid-free HR2 peptides were never identified on cells (negative data not shown). By contrast, cholesterol-HR2 peptides, after incubation with cells for 30 min at 37 °C, were detected inside cells, as definite puncta, and partially colocalizing with cholera toxin B (CTB), a marker for lipid raft-associated ganglioside GM1 (Fig. 5F, white arrow). Similar results were observed using biotinylated palmitate-HR2 peptides (data not shown). Collectively, these results demonstrated that the cholesterol or palmitate adducts allowed the antiviral peptides to access endosomes and prevent virus fusion out of endosomes.

2.4. Effects of high protease levels on MERS entry and resistance to HR2 peptides

The previous findings demonstrated that MERS pps can avoid untagged HR2 peptides by delaying their fusion triggering to times after endocytosis. We speculated that MERS pps proceeding through fusion triggering with very little delay might also escape HR2 peptides, because their fusion intermediates come and go too quickly for HR2-mediated intervention. Very high cell-surface protease levels will accelerate CoV-cell entry (Shirato et al., 2016). We hypothesized that a protease-accelerated cell entry process might escape suppressive HR2 effects, but we questioned whether lipid-conjugated HR2 peptides might capture and block the fast-entering viruses.

To address this question, we first determined the pace of MERS pp entry into Caco2 cells. To measure entry kinetics, MERS pps were allowed to enter cells for defined periods, and then halted from further entry by adding a protease inhibitor cocktail. The extents of transduction before inhibitor-arrest were then determined 18 h later. In Caco2 cells, which express endogenous TMPR serine proteases, 50% of MERS transduction was acquired by 20 min after 37 °C incubation (Fig. 6A, solid line). TMPRSS2 overexpression accelerated virus entry by 5 min (Fig. 6A, dashed line), while inactivating endogenous TMPR serine proteases with camostat decelerated virus entry by 40 min (Fig. 6A, dotted line). These results were consistent with a recent report on HCoV-229E virus entry kinetics (Shirato et al., 2016).

In assessing the relationships between entry kinetics and HR2 sensitivity, we found that the unconjugated, as well as tocopherol- and palmitate-conjugated HR2 peptides remained equally antiviral to fast or slow-entering viruses (Fig. 6B-E), with the palmitate-HR2 being most antiviral. Notably, the cholesterol-conjugated HR2 showed some differential antiviral activities, being relatively ineffective at blocking the fast-entering MERS pps (Fig. 6D). These results indicate that virus entry can escape cholesterol-HR2 through rapid entry, but that other lipid tags, notably palmitate, can position HR2s to arrest these quick-acting viruses.

3. Discussion

Enveloped virus fusion-blocking peptides have been evaluated for the past 25 years as candidate antiviral agents (Jiang et al., 1993; Lambert et al., 1996; Rapaport et al., 1995; Wild et al., 1994; Young et al., 1997). From these studies, it has become clear that the peptides bind and inactivate viral envelope proteins when they are in their transient, "extended" fusion intermediate states (Kielian and Rey, 2006; Netter et al., 2004). Depending on the infecting virus, these intermediates appear shortly after virus-receptor binding, or they may appear much later, after viruses have been engulfed inside endosomes. Once formed, the intermediates may quickly induce fusion and zip into post-fusion structures, or they may remain for prolonged periods as they wait for adjacent fusion intermediates to accumulate and then cooperate in membrane coalescence and compression into post-fusion forms (Ivanovic and Harrison, 2015). For example, during HIV entry, envelope proteins convert from pre-fusion to fusion-intermediate forms, and then remain in such forms for extended periods, until a time that they join with neighboring intermediates and cooperatively pull membranes together. This makes for relatively long-lived fusion intermediates that are durable targets for fusion inhibitory peptides (Reeves et al., 2002). Contrastingly, during influenza entry, envelope proteins convert from pre-fusion to intermediate forms at relatively late times, after virus endocytosis, and then cooperatively transit quickly into post-fusion states. This makes for short-lived, endosome-restricted fusion intermediates that are poorly targeted by fusion inhibitory peptides (Shen et al., 2013; Xu and Wilson, 2011).

The CoVs are set apart from the HIV and influenza cases by their variable cell entry routes, both rapid, likely cell-surface routes and slower, definitively endosomal routes, depending on the time and place of protease-directed fusion triggering (Millet and Whittaker, 2015). This makes for CoV fusion intermediates with different dwell times and

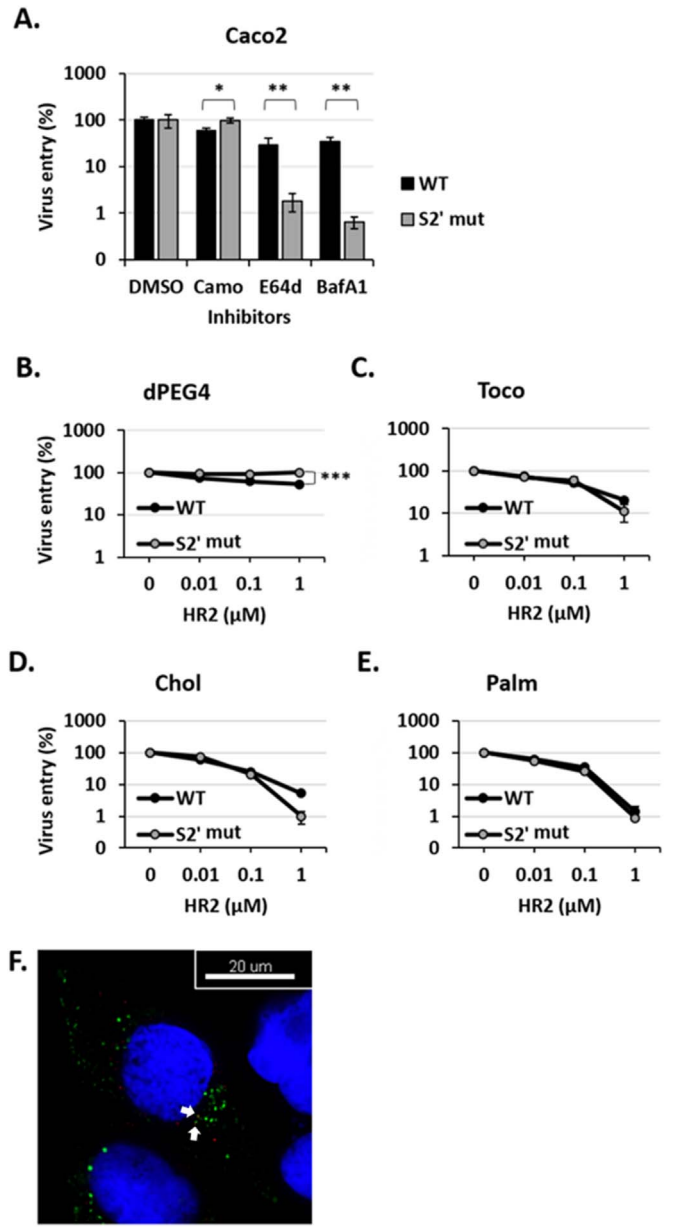

Fig. 5. Inhibition of endosome-localized MERS entry by lipid-conjugated HR2 peptides. (A) Caco2 cells were incubated with DMSO, 100 μM camostat (Camo), 10 μM E64d, or 100 nM bafilomycin A1 (BafA1) for 1 h, then transduced with WT or S2′ mutant (S2′ mut) MERS pps, without removing previously applied inhibitors. (B-E) Caco2 cells were transduced with WT or S2′ mut MERS pps in the presence of increasing concentrations of dPEG4 (B), tocopherol (C), cholesterol (D), or palmitate (E) tagged HR2 peptides. After 1 h, unbound MERS pps and entry inhibitors were removed. Virus entry was quantified by measuring luciferase levels at 48 h post-transduction. Error bars present SD from the mean (n = 3). Statistical significance was assessed by student's *t*-test. *, P < 0.05; **, P < 0.01; ***, P < 0.001. (F) Caco2 cells were incubated with biotinylated cholesterol-HR2 peptides at 37 °C for 30 min. Cells then were stained for biotinylated HR2 peptide (in red), ganglioside GM1 (in green), and nuclei (in blue). The white arrows point to punctae of colocalizing HR2 peptide and ganglioside GM1.

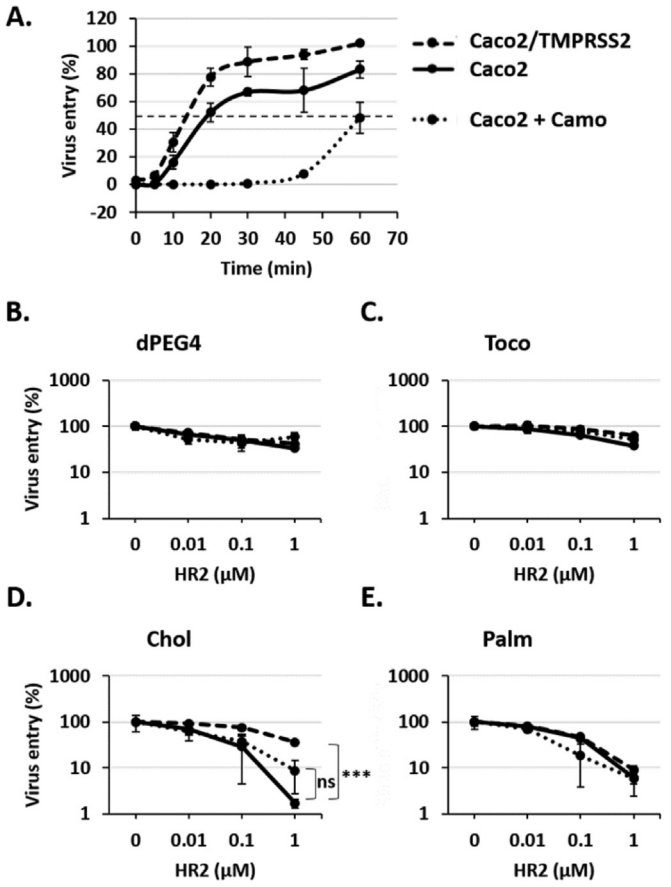

Fig. 6. Effects of high protease levels on MERS entry and resistance to antiviral HR2 peptides. (A) Caco2 cells were transduced with Ad5-hTMPRSS2 (Caco2/TMPRSS2), or incubated with 100 μM camostat (Caco2+Camo). Cells then were incubated with MERS pps at 4 °C for 1 h, then shifted to 37 °C at time = 0. At the indicated time points after 37 °C shift, cells were treated with an entry inhibitor cocktail (100 μM camostat, 10 μM dec-RVKR-cmk, 10 μM E64d). (B–E) Caco2, Caco2/TMPRSS2, and Caco2+Camo cells were transduced with MERS pps in the presence of the indicated HR2 peptides. Virus entry was quantified by measuring luciferase levels at 18 h (A) or 48 h (B-E) post-transduction. Error bars present SD from the mean (n = 3). Statistical significance was assessed by student's *t*-test. ***, P < 0.001; ns, not significant.

different subcellular locations. Furthermore, the targets of fusion inhibitory peptides on CoV S proteins show considerable variety (Fig. 1B), and they can even diversify into structures that are resistant to soluble HR2 peptides (Bosch et al., 2008b). Therefore, it was impressive that we found a single inhibitory peptide, MERS HR2-palmitate, and to a slightly lesser extent MERS HR2-cholesterol, blocking so many different CoV S-mediated cell entry processes (Fig. 2). This broad anti-CoV activity was attributed to the lipid moieties, which we claim are placing the HR2 peptides at or near fusion-triggering proteases. Cholesterol and palmitate associate with lipid rafts (Schumann et al., 2011), which are enriched with the receptors and proteases that activate MERS-CoV S (Andre et al., 2006; Earnest et al., 2015; Le Naour et al., 2006; Rana et al., 2011). Generally, cholesterol- and palmitate- adducts increased HR2 antiviral activity, whereas tocopherol did not (Figs. 2 and 4). α-Tocopherol is thought to incorporate into PUFA-rich non-raft domains (Atkinson et al., 2010; Raederstorff et al., 2015), a location that we contend is distant from the CoV fusion-triggering proteases. These findings add to several formative reports demonstrating that lipid tags increase antiviral activities of fusion-blocking peptides (Lee et al., 2011; Porotto et al., 2010) and they suggest that a single lipidated HR2 peptide can suppress a wide range of pathogenic CoVs, even those that have acquired adaptive mutations in their S protein fusion domains (Cotten et al., 2014; Kim et al., 2016; Scobey et al., 2013).

Cholesterol- and palmitate- conjugated HR2 peptides also inhibited the relatively slow MERS-CoV S-mediated entry that takes place in endosomes (Figs. 4 and 5), suggesting that these two lipids tether HR2 peptides near viruses throughout their endocytosis. That lipid conjugations allow HR2 peptides to accumulate in endosomes, thereby blocking “slow”-entering viruses, has been recently documented (Figueira et al., 2016; Lee et al., 2011), and is again shown here with the CoVs. However, when the virus entry was accelerated, through TMPRSS2 overexpression, the cholesterol-conjugated HR2 lost much

of its antiviral potential (Fig. 6D), while the palmitate-conjugated HR2 did not (Fig. 6E). This may be explained by a broader distribution of palmitate-HR2 on cell surfaces, or a greater capacity for palmitate-HR2 to diffuse rapidly on cell membranes, such that it can quickly engage and inactivate the "fast"-operating viral fusion intermediates. Many CoVs appear to take a fast cell entry route; indeed, HR2 peptides inhibited MHV only within a 5- to 15-min postinfection time period (Shulla and Gallagher, 2009), indicating a cell entry process that is significantly more rapid than that of HIV (~ 75 min) or avian sarcoma and leucosis virus subgroup A (~ 45 min) (Munoz-Barroso et al., 1998; Netter et al., 2004). To block both fast and slow-entering CoVs, the palmitate-conjugated HR2 peptides appear to be the superior choice.

The findings in this report also argue that fusion-triggering proteases, by cleaving S proteins at the S2-prime location, will release constraints and allow S proteins to convert into the intermediates that are targeted by HR2 peptides. Previous reports suggested this to be the case (Matsuyama et al., 2010; Ujike et al., 2008), but have not provided definitive evidence. Here we consistently observed direct correlations between cell-surface, virus-activating proteases and HR2 antiviral potencies (Fig. 3). Without the S2-prime cleavage substrate, MERS S proteins did not acquire susceptibility to soluble (lipid-free) HR2 peptides (Fig. 5B). These findings indicate that proteolysis at the S2-prime position is required to form HR2-sensitive S protein structures.

The importance of the proteolysis at S2-prime is also evident from S protein structures. The atomic-resolution structures of native CoV S proteins (Kirchdoerfer et al., 2016; Walls et al., 2016a, 2016b) reveal a complex, folded, and buried set of four consecutive helices that comprise the site to which antiviral HR2 peptides bind. They are held in place, in part, through their interactions with domains that are distal to the virion. In the available post-fusion S protein structures, this HR2 binding site is a continuous helical trimer, with HR2 embedded into interhelical grooves (Gao et al., 2013; Lu et al., 2014). While the details of the conversion from pre-fusion to fusion-intermediate states are unknown, it is obvious that fairly dramatic conformational changes would be required to release these helices and allow for intervening loop-to-helix transitions, such that a linear helical trimer can form. Current proposed events include receptor-directed stabilization of alternative S protein conformations (Gui et al., 2017), which may facilitate exposure of the S2-prime cleavage sites (Walls et al., 2016b). Subsequently, S2-prime cleavage would be expected to liberate the bundle of short helices and loops such that it can extend into a long helical trimer.

In this report, we have identified relationships between proteases, virus-cell entry kinetics, and HR2 peptide-mediated antiviral activities. The likelihood that HR2 peptides will prevent CoV-cell entry depends on the protease-directed timing and location of S protein conversion into fusion intermediates. HR2 peptides have difficulty accessing fusion intermediates that are short-lived, or long-lived but deep within endosomes. Lipid tags on the HR2 peptides can position HR2s on cells, such that they more readily bind to these intermediates and provide a broader and more potent antiviral effect. A final note here is that serine protease inhibitors are being considered as potential antiviral drugs suppressing CoV (Kawase et al., 2012; Zhou et al., 2015), and influenza (Bahgat et al., 2011; Zhou et al., 2015). It appears that inhibitors of cell-surface serine proteases can drive CoVs to the slow, endosomal entry routes in which lipid-free HR2 peptides have no antiviral activities. This finding has implications for the use of protease inhibitors and fusion-inhibiting peptides in combination, and argues that lipidated HR2 peptides are a sensible choice for future combination therapies.

4. Materials and methods

4.1. Cells

HEK293 cells were maintained in 293T media (Dulbecco's Modified Eagle Media [DMEM] supplemented with 10% fetal bovine serum [FBS, Atlanta Biologicals, Norcross, GA], 10 mM HEPES, 100 mM sodium pyruvate, 0.1 mM non-essential amino acids, and 100 U/ml penicillin-streptomycin). Calu3 and Caco2 cells were maintained in Minimum Essential Media (MEM) supplemented with 20% FBS, 100 U/ml penicillin-streptomycin. Huh7 cells were maintained in DMEM supplemented with 10% FBS, 10 mM HEPES, 0.1 mM non-essential amino acids, and 100 U/ml penicillin-streptomycin. Vero81 cells were maintained in DMEM supplemented with 10% FBS, 100 U/ml penicillin G, and 100 μg/ml streptomycin. Delayed brain tumor (DBT) cells were maintained in MEM supplemented with 5% FBS, 10% tryptose phosphate broth, 2 mM L-glutamine, and 100 U/ml penicillin-streptomycin. Cell culture materials and reagents were obtained from Corning Inc. (Corning, NY) and Hyclone (Logan, UT) unless otherwise noted.

4.2. Viruses

Recombinant MHV-A59 containing a Fluc reporter gene was produced and propagated on DBT cells as described previously (Shulla and Gallagher, 2009). Virus entry was measured by Fluc assay at 5 h post-infection.

4.3. Plasmids

DNA encoding codon-optimized MERS-CoV EMC/2012 S (GenBank accession number JX869059) containing a C-terminal C9 tag (pcDNA3.1-MERS S-C9) was purchased from GenScript Inc. (Piscataway, NJ). For the generation of cleavage site mutant MERS-CoV, MERS S-C9 was PCR-amplified with mutagenic primers (Table 1), and PCR fragments were assembled using Gibson Assembly (NEB, Ipswich, SD). All constructs were confirmed by Sanger sequence analysis. Plasmid encoding C-terminal flag-tagged human DPP4 (GenBank accession no. NM_001935, pCMV6-Entry-hDPP4) was purchased from OriGene (Rockville, MD). pcDNA3.1-SARS-S-C9 and pcDNA3.1-hACE2-C9 plasmids were provided by Michael Farzan, Scripps Research Institute. pcDNA3.1-229E-S-C9 and pcDNA3.1-hAPN plasmids were provided by Fang Li, University of Minnesota. pCAGGS-MHV-S (A59 strain) and pcDNA3.1-mCEACAM were previously constructed (Boscarino et al., 2008). pHEF-VSV G was provided from BEI resources (Manassas, VA). pcDNA3.1-TMPRSS2-flag was previously constructed (Shulla et al., 2011). pNL4.3-Luc R- E-was obtained from the NIH AIDS Research and Reference Program, cat # 3418.

4.4. HIV pseudoparticle (pp) preparation

To produce HIV pps, HEK293 cells were transfected with pNL4.3-Luc R-E- in conjunction with plasmids encoding MERS-CoV S, SARS-CoV S, HCoV-229E S, MHV S, or VSV G using polyethylenimine (PEI, Polysciences Inc., Warrington, PA). Cell-free supernatants containing pps were collected at 48 h post-transfection, filtered through 0.45 μm syringe filters (Pall Life Sciences, Port Washington, NY), and stored at − 80 °C until use. All pseudoviruses were normalized for transducing activities by titration on HEK293 cells expressing appropriate CoV receptors, and were normalized for particle concentration by western blotting using HIV p24 antibodies.

Table 1
Primers for the generation of cleavage site mutant MERS pps.

Primer name	Primer sequences
S2′ mut F	5′ ACAGGCAGTTCGAGCTATGGCAGCGCAATC 3′
S2′ mut R	5′ GATTGCGCTGCCATAGCTCGAACTGCCTGT 3′
M13_pUC F	5′ CCTGTGTGAAATTGTTATCCGCTCAC 3′
M13_pUC R	5′ GTGAGCGGATAACAATTTCACACAGG 3′

4.5. HIV pp transductions

Target cells were transduced at equivalent input multiplicities for 1 h at 37 °C, subsequently washed, and incubated for an additional 48 h. Where indicated, cells were transfected with DPP4, ACE2, APN, CEACAM1a, TMPRSS2-flag using PEI at 48 h before transduction. Where indicated, cells were incubated with indicated concentrations of camostat, E64d, bafilomycin A1 (all from Sigma-Aldrich Corporation) at 1 h before transduction, and then transduced with pps without removing previously applied inhibitors. At the end of transduction periods, cells were dissolved in cell culture lysis buffer (25 mM Tris-phosphate [pH 7.8], 2 mM DTT, 2 mM 1,2-diaminocyclohexane-N,N,N′,N′-tetraacetic acid, 10% glycerol, 1% Triton X-100) and luciferase levels were measured by addition of Fluc substrate (1 mM D-luciferin, 3 mM ATP, 15 mM MgSO4·H2O, 30 mM HEPES [pH 7.8]) using a Veritas microplate luminometer (Turner BioSystems, Sunnyvale, CA).

4.6. HR2 peptide

The MERS-CoV HR2 peptide (SLTQINTTLLDLTYEMLSLQQVV KALNESYIDLKEL, aa 1251–1286) was designed as described previously (Lu et al., 2014). Lipid-free and lipid-tagged HR2 peptides were synthesized from American Peptide Company, Inc. (Sunnyvale, CA) and kindly obtained from Dr. Matteo Porotto, Department of Pediatrics, Columbia University. HPLC analyses of each HR2 peptide preparation revealed single uniform peaks reflecting > 99% lipopeptide purities. HR2 peptides were dissolved in DMSO and kept at − 80 °C. Cells were incubated with serially diluted HR2 peptides for 1 h at 37 °C and then incubated with pps or MHV-A59 without removing previously applied HR2 peptides.

4.7. Detection of biotinylated HR2 peptides

For biotinylation of HR2 peptide, 1 μM cholesterol tagged HR2 peptides were incubated with 20 μM EZ-Link Sulfo-NHS-Biotin (Pierce, Rockford, IL) for 30 min at room temperature. Reactions were quenched with glycine. Free biotins were removed using PlusOne Mini Dialysis Kit reagents (Amersham Biosciences, San Francisco, CA).

Caco2 cells were incubated with 1 μM biotinylated HR2 peptides at 37 °C. After 30 min, cells were fixed, permeablized, and stained for HR2 peptides and ganglioside G_{m1} using APC conjugated streptavidin (Southern Biotech, Birmingham, AL) and Alexa Fluor 555 conjugated CTB (Invitrogen, Grand Island, NY), respectively. Cell nuclei were stained with Hoechst 33258 (Invitrogen). The cells were imaged with a DeltaVision microscope (Applied Precision) equipped with a digital camera (CoolSNAP HQ; Photometrics), using a 1.4-numerical-aperture 100 × lens objective. Images were deconvolved with SoftWoRx deconvolution software (Applied Precision) analyzed using Imaris version 6.3.1 (Bitplane Scientific Solutions).

4.8. Entry kinetics assay

VSV-based pps were generated as described previously (Park et al., 2016). Briefly, HEK293 cells were transfected with MERS S-C9 using PEI. At 24 h post-transfection, cells were incubated with VSVluc-ΔVSVG complemented with Junin virus glycoproteins for 1 h. Cells were then rinsed three times with media. Cell-free supernatants containing pps were collected at 48 h post-transfection, filtered through 0.45 μm syringe filters (Pall Life Sciences, Port Washington, NY), and stored at −80 °C until use.

For entry kinetics assays, cells were incubated with VSV based pps for 1 h at 4 °C. Unbound pps were then removed and cells shifted to 37 °C. At indicated time points after 37 °C shift, cells were treated with protease inhibitor cocktail (100 μM camostat, 10 μM dec-RVKR-cmk, 10 μM E64d). At 18 h post-transduction, virus entry was measured by Fluc assay.

Table 2
Primers for real-time PCR.

Target mRNA	Primer name	Primer sequences
DPP4	DPP4 F	5′ TACAAAAGTGACATGCCTCAGTT 3′
	DPP4 R	5′ TGTGTAGAGTATAGAGGGGCAGA 3′
TMPRSS2	TMPRSS2 F	5′ CTCTACGGACCAAACTTCATC 3′
	TMPRSS2 R	5′ CCACTATTCCTTGGCTAGAGTA 3′
Furin	Furin F	5′ CCTGGTTGCTATGGGTGGTAG 3′
	Furin R	5′ AAGTGGTAATAGTCCCCGAAGA 3′
Cathepsin L	CTSL F	5′ GTGGACATCCCTAAGCAGGA 3′
	CTSL R	5′ CACAATGGTTTCTCCGGTC 3′
HPRT	HPRT F	5′ CTCGTTCTCTTGCAGAACTTTG 3′
	HPRT R	5′ TGCCCAGGTGGAAAGGT 3′

4.9. Real time PCR

Total RNA was extracted from Vero81, Huh7, Caco2, and Calu3 cells using a Qiagen RNeasy mini kit according to the manufacturer's instructions. A total of 500 ng RNA was reverse transcribed using the Thermo Scientific RevertAid RT kit (Waltham, MA). Real-time PCR was performed to quantify mRNA expression levels of DPP4, TMPRSS2, furin, cathepsin L, and hypoxanthine-guanine phosphoribosyltransferase (HPRT) using the primers described in Table 2 and RT^2 SYBR Green qPCR Mastermix (Qiagen). Expression data were normalized to the geometric mean of the housekeeping gene HPRT and calculated with the ddCt method.

4.10. Statistical analyses

All experiments were independently repeated at least three times. Data are presented as mean ± standard deviation (SD). Statistical significance was calculated using the Holm-Sidak multiple Student's *t*-test procedure. A P value of < 0.05 was considered statistically significant.

Acknowledgements

We especially thank Matteo Porotto (Columbia University) for providing lipidated HR2 peptide reagents and for helpful discussions throughout this project. James Earnest, Arlene Barlan, Steve Ollosi, and Joseph Westrich (all at Loyola University) also provided valuable input and technical support. Financial support was provided by the Falk Foundation and by the National Institutes of Health (NIH grant P01 AI 060699 to Stanley Perlman, University of Iowa).

References

Andre, M., Le Caer, J.P., Greco, C., Planchon, S., El Nemer, W., Boucheix, C., Rubinstein, E., Chamot-Rooke, J., Le Naour, F., 2006. Proteomic analysis of the tetraspanin web using LC-ESI-MS/MS and MALDI-FTICR-MS. Proteomics 6, 1437–1449.

Annan, A., Baldwin, H.J., Corman, V.M., Klose, S.M., Owusu, M., Nkrumah, E.E., Badu, E.K., Anti, P., Agbenyega, O., Meyer, B., Oppong, S., Sarkodie, Y.A., Kalko, E.K., Lina, P.H., Godlevska, E.V., Reusken, C., Seebens, A., Gloza-Rausch, F., Vallo, P., Tschapka, M., Drosten, C., Drexler, J.F., 2013. Human betacoronavirus 2c EMC/2012-related viruses in bats, Ghana and Europe. Emerg. Infect. Dis. 19, 456–459.

Anthony, S.J., Gilardi, K., Menachery, V.D., Goldstein, T., Ssebide, B., Mbabazi, R., Navarrete-Macias, I., Liang, E., Wells, H., Hicks, A., Petrosov, A., Byarugaba, D.K., Debbink, K., Dinnon, K.H., Scobey, T., Randell, S.H., Yount, B.L., Cranfield, M., Johnson, C.K., Baric, R.S., Lipkin, W.I., Mazet, J.A., 2017. Further evidence for bats as the evolutionary source of middle east respiratory syndrome coronavirus. MBio, 8. http://dx.doi.org/10.1128/mBio.00373-17.

Atkinson, J., Harroun, T., Wassall, S.R., Stillwell, W., Katsaras, J., 2010. The location and behavior of alpha-tocopherol in membranes. Mol. Nutr. Food Res. 54, 641–651.

Bahgat, M.M., Blazejewska, P., Schughart, K., 2011. Inhibition of lung serine proteases in mice: a potentially new approach to control influenza infection. Virol. J. 8, 27.

Belouzard, S., Chu, V.C., Whittaker, G.R., 2009. Activation of the SARS coronavirus spike protein via sequential proteolytic cleavage at two distinct sites. Proc. Natl. Acad. Sci. Usa. 106, 5871–5876.

Belouzard, S., Millet, J.K., Licitra, B.N., Whittaker, G.R., 2012. Mechanisms of coronavirus cell entry mediated by the viral spike protein. Viruses 4, 1011–1033.

Boscarino, J.A., Logan, H.L., Lacny, J.J., Gallagher, T.M., 2008. Envelope protein

palmitoylations are crucial for murine coronavirus assembly. J. Virol. 82, 2989–2999.
Bosch, B.J., Bartelink, W., Rottier, P.J., 2008a. Cathepsin L functionally cleaves the severe acute respiratory syndrome coronavirus class I fusion protein upstream of rather than adjacent to the fusion peptide. J. Virol. 82, 8887–8890.
Bosch, B.J., Martina, B.E., Van Der Zee, R., Lepault, J., Haijema, B.J., Versluis, C., Heck, A.J., De Groot, R., Osterhaus, A.D., Rottier, P.J., 2004. Severe acute respiratory syndrome coronavirus (SARS-CoV) infection inhibition using spike protein heptad repeat-derived peptides. Proc. Natl. Acad. Sci. Usa. 101, 8455–8460.
Bosch, B.J., Rossen, J.W., Bartelink, W., Zuurveen, S.J., de Haan, C.A., Duquerroy, S., Boucher, C.A., Rottier, P.J., 2008b. Coronavirus escape from heptad repeat 2 (HR2)-derived peptide entry inhibition as a result of mutations in the HR1 domain of the spike fusion protein. J. Virol. 82, 2580–2585.
Bosch, B.J., van der Zee, R., de Haan, C.A., Rottier, P.J., 2003. The coronavirus spike protein is a class I virus fusion protein: structural and functional characterization of the fusion core complex. J. Virol. 77, 8801–8811.
Channappanavar, R., Lu, L., Xia, S., Du, L., Meyerholz, D.K., Perlman, S., Jiang, S., 2015. Protective effect of intranasal regimens containing peptidic Middle East Respiratory syndrome coronavirus fusion inhibitor against MERS-CoV infection. J. Infect. Dis. 212, 1894–1903.
Channappanavar, R., Perlman, S., 2017. Pathogenic human coronavirus infections: causes and consequences of cytokine storm and immunopathology. Semin. Immunopathol..
Choi, K.S., Aizaki, H., Lai, M.M., 2005. Murine coronavirus requires lipid rafts for virus entry and cell-cell fusion but not for virus release. J. Virol. 79, 9862–9871.
Cotten, M., Watson, S.J., Zumla, A.I., Makhdoom, H.Q., Palser, A.L., Ong, S.H., Al Rabeeah, A.A., Alhakeem, R.F., Assiri, A., Al-Tawfiq, J.A., Albarrak, A., Barry, M., Shibl, A., Alrabiah, F.A., Hajjar, S., Balkhy, H.H., Flemban, H., Rambaut, A., Kellam, P., Memish, Z.A., 2014. Spread, circulation, and evolution of the Middle East respiratory syndrome coronavirus. MBio, 5. http://dx.doi.org/10.1128/mBio.01062-13.
de Wit, E., van Doremalen, N., Falzarano, D., Munster, V.J., 2016. SARS and MERS: recent insights into emerging coronaviruses. Nat. Rev. Microbiol. 14, 523–534.
Earnest, J.T., Hantak, M.P., Park, J.E., Gallagher, T., 2015. Coronavirus and influenza virus proteolytic priming takes place in tetraspanin-enriched membrane microdomains. J. Virol. 89, 6093–6104.
Figueira, T.N., Palermo, L.M., Veiga, A.S., Huey, D., Alabi, C.A., Santos, N.C., Welsch, J.C., Mathieu, C., Horvat, B., Niewiesk, S., Moscona, A., Castanho, M.A., Porotto, M., 2016. In vivo efficacy of measles virus fusion protein-derived peptides is modulated by properties of self-assembly and membrane residence. J. Virol..
Gao, J., Lu, G., Qi, J., Li, Y., Wu, Y., Deng, Y., Geng, H., Li, H., Wang, Q., Xiao, H., Tan, W., Yan, J., Gao, G.F., 2013. Structure of the fusion core and inhibition of fusion by a heptad repeat peptide derived from the S protein of Middle East respiratory syndrome coronavirus. J. Virol. 87, 13134–13140.
Gierer, S., Bertram, S., Kaup, F., Wrensch, F., Heurich, A., Kramer-Kuhl, A., Welsch, K., Winkler, M., Meyer, B., Drosten, C., Dittmer, U., von Hahn, T., Simmons, G., Hofmann, H., Pohlmann, S., 2013. The spike protein of the emerging betacoronavirus EMC uses a novel coronavirus receptor for entry, can be activated by TMPRSS2, and is targeted by neutralizing antibodies. J. Virol. 87, 5502–5511.
Graham, R.L., Donaldson, E.F., Baric, R.S., 2013. A decade after SARS: strategies for controlling emerging coronaviruses. Nat. Rev. Microbiol. 11, 836–848.
Gui, M., Song, W., Zhou, H., Xu, J., Chen, S., Xiang, Y., Wang, X., 2017. Cryo-electron microscopy structures of the SARS-CoV spike glycoprotein reveal a prerequisite conformational state for receptor binding. Cell Res. 27, 119–129.
Hrobowski, Y.M., Garry, R.F., Michael, S.F., 2005. Peptide inhibitors of dengue virus and West Nile virus infectivity. Virol. J. 2, 49.
Ivanovic, T., Harrison, S.C., 2015. Distinct functional determinants of influenza hemagglutinin-mediated membrane fusion. Elife 4, e11009.
Jiang, S., Lin, K., Strick, N., Neurath, A.R., 1993. HIV-1 inhibition by a peptide. Nature 365, 113.
Kawase, M., Shirato, K., Matsuyama, S., Taguchi, F., 2009. Protease-mediated entry via the endosome of human coronavirus 229E. J. Virol. 83, 712–721.
Kawase, M., Shirato, K., van der Hoek, L., Taguchi, F., Matsuyama, S., 2012. Simultaneous treatment of human bronchial epithelial cells with serine and cysteine protease inhibitors prevents severe acute respiratory syndrome coronavirus entry. J. Virol. 86, 6537–6545.
Kielian, M., Rey, F.A., 2006. Virus membrane-fusion proteins: more than one way to make a hairpin. Nat. Rev. Microbiol. 4, 67–76.
Kim, Y., Cheon, S., Min, C.K., Sohn, K.M., Kang, Y.J., Cha, Y.J., Kang, J.I., Han, S.K., Ha, N.Y., Kim, G., Aigerim, A., Shin, H.M., Choi, M.S., Kim, S., Cho, H.S., Kim, Y.S., Cho, N.H., 2016. Spread of mutant middle east respiratory syndrome coronavirus with reduced affinity to human CD26 during the South Korean outbreak. MBio, 7. http://dx.doi.org/10.1128/mBio.00019-16.
Kirchdoerfer, R.N., Cottrell, C.A., Wang, N., Pallesen, J., Yassine, H.M., Turner, H.L., Corbett, K.S., Graham, B.S., McLellan, J.S., Ward, A.B., 2016. Pre-fusion structure of a human coronavirus spike protein. Nature 531, 118–121.
Lambert, D.M., Barney, S., Lambert, A.L., Guthrie, K., Medinas, R., Davis, D.E., Bucy, T., Erickson, J., Merutka, G., Petteway, S.R., Jr, 1996. Peptides from conserved regions of paramyxovirus fusion (F) proteins are potent inhibitors of viral fusion. Proc. Natl. Acad. Sci. USA 93, 2186–2191.
Lau, S.K., Woo, P.C., Li, K.S., Huang, Y., Tsoi, H.W., Wong, B.H., Wong, S.S., Leung, S.Y., Chan, K.H., Yuen, K.Y., 2005. Severe acute respiratory syndrome coronavirus-like virus in Chinese horseshoe bats. Proc. Natl. Acad. Sci. USA 102, 14040–14045.
Le Naour, F., Andre, M., Boucheix, C., Rubinstein, E., 2006. Membrane microdomains and proteomics: lessons from tetraspanin microdomains and comparison with lipid rafts. Proteomics 6, 6447–6454.
Lee, K.K., Pessi, A., Gui, L., Santoprete, A., Talekar, A., Moscona, A., Porotto, M., 2011. Capturing a fusion intermediate of influenza hemagglutinin with a cholesterol-conjugated peptide, a new antiviral strategy for influenza virus. J. Biol. Chem. 286, 42141–42149.
Li, W., Moore, M.J., Vasilieva, N., Sui, J., Wong, S.K., Berne, M.A., Somasundaran, M., Sullivan, J.L., Luzuriaga, K., Greenough, T.C., Choe, H., Farzan, M., 2003. Angiotensin-converting enzyme 2 is a functional receptor for the SARS coronavirus. Nature 426, 450–454.
Li, W., Shi, Z., Yu, M., Ren, W., Smith, C., Epstein, J.H., Wang, H., Crameri, G., Hu, Z., Zhang, H., Zhang, J., McEachern, J., Field, H., Daszak, P., Eaton, B.T., Zhang, S., Wang, L.F., 2005. Bats are natural reservoirs of SARS-like coronaviruses. 310, 676–679.
Liu, I.J., Tsai, W.T., Hsieh, L.E., Chueh, L.L., 2013. Peptides corresponding to the predicted heptad repeat 2 domain of the feline coronavirus spike protein are potent inhibitors of viral infection. PLoS One 8, e82081.
Lu, L., Liu, Q., Zhu, Y., Chan, K.H., Qin, L., Li, Y., Wang, Q., Chan, J.F., Du, L., Yu, F., Ma, C., Ye, S., Yuen, K.Y., Zhang, R., Jiang, S., 2014. Structure-based discovery of Middle East respiratory syndrome coronavirus fusion inhibitor. Nat. Commun. 5, 3067.
Lu, Y., Liu, D.X., Tam, J.P., 2008. Lipid rafts are involved in SARS-CoV entry into Vero E6 cells. Biochem. Biophys. Res. Commun. 369, 344–349.
Matsuyama, S., Nagata, N., Shirato, K., Kawase, M., Takeda, M., Taguchi, F., 2010. Efficient activation of the severe acute respiratory syndrome coronavirus spike protein by the transmembrane protease TMPRSS2. J. Virol. 84, 12658–12664.
Matsuyama, S., Taguchi, F., 2009. Two-step conformational changes in a coronavirus envelope glycoprotein mediated by receptor binding and proteolysis. J. Virol. 83, 11133–11141.
Matsuyama, S., Ujike, M., Ishii, K., Fukushi, S., Morikawa, S., Tashiro, M., Taguchi, F., 2006. Enhancement of SARS-CoV infection by proteases. Adv. Exp. Med. Biol. 581, 253–258.
McReynolds, S., Jiang, S., Guo, Y., Celigoy, J., Schar, C., Rong, L., Caffrey, M., 2008. Characterization of the prefusion and transition states of severe acute respiratory syndrome coronavirus S2-HR2. Biochemistry 47, 6802–6808.
Memish, Z.A., Cotten, M., Meyer, B., Watson, S.J., Alsahafi, A.J., Al Rabeeah, A.A., Corman, V.M., Sieberg, A., Makhdoom, H.Q., Assiri, A., Al Masri, M., Aldabbagh, S., Bosch, B.J., Beer, M., Muller, M.A., Kellam, P., Drosten, C., 2014. Human infection with MERS coronavirus after exposure to infected camels, Saudi Arabia, 2013. Emerg. Infect. Dis. 20, 1012–1015.
Millet, J.K., Whittaker, G.R., 2015. Host cell proteases: critical determinants of coronavirus tropism and pathogenesis. Virus Res. 202, 120–134.
Millet, J.K., Whittaker, G.R., 2014. Host cell entry of Middle East respiratory syndrome coronavirus after two-step, furin-mediated activation of the spike protein. Proc. Natl. Acad. Sci. USA 111, 15214–15219.
Munoz-Barroso, I., Durell, S., Sakaguchi, K., Appella, E., Blumenthal, R., 1998. Dilation of the human immunodeficiency virus-1 envelope glycoprotein fusion pore revealed by the inhibitory action of a synthetic peptide from gp41. J. Cell Biol. 140, 315–323.
Netter, R.C., Amberg, S.M., Balliet, J.W., Biscone, M.J., Vermeulen, A., Earp, L.J., White, J.M., Bates, P., 2004. Heptad repeat 2-based peptides inhibit avian sarcoma and leukosis virus subgroup a infection and identify a fusion intermediate. J. Virol. 78, 13430–13439.
Nomura, R., Kiyota, A., Suzaki, E., Kataoka, K., Ohe, Y., Miyamoto, K., Senda, T., Fujimoto, T., 2004. Human coronavirus 229E binds to CD13 in rafts and enters the cell through caveolae. J. Virol. 78, 8701–8708.
Park, J.E., Li, K., Barlan, A., Fehr, A.R., Perlman, S., McCray, P.B., Jr, Gallagher, T., 2016. Proteolytic processing of Middle East respiratory syndrome coronavirus spikes expands virus tropism. Proc. Natl. Acad. Sci. USA 113, 12262–12267.
Porotto, M., Yokoyama, C.C., Palermo, L.M., Mungall, B., Aljofan, M., Cortese, R., Pessi, A., Moscona, A., 2010. Viral entry inhibitors targeted to the membrane site of action. J. Virol. 84, 6760–6768.
Qian, Z., Dominguez, S.R., Holmes, K.V., 2013. Role of the spike glycoprotein of human Middle East respiratory syndrome coronavirus (MERS-CoV) in virus entry and syncytia formation. PLoS One 8, e76469.
Qiu, Z., Hingley, S.T., Simmons, G., Yu, C., Das Sarma, J., Bates, P., Weiss, S.R., 2006. Endosomal proteolysis by cathepsins is necessary for murine coronavirus mouse hepatitis virus type 2 spike-mediated entry. J. Virol. 80, 5768–5776.
Raederstorff, D., Wyss, A., Calder, P.C., Weber, P., Eggersdorfer, M., 2015. Vitamin E function and requirements in relation to PUFA. Br. J. Nutr. 114, 1113–1122.
Raj, V.S., Mou, H., Smits, S.L., Dekkers, D.H., Muller, M.A., Dijkman, R., Muth, D., Demmers, J.A., Zaki, A., Fouchier, R.A., Thiel, V., Drosten, C., Rottier, P.J., Osterhaus, A.D., Bosch, B.J., Haagmans, B.L., 2013. Dipeptidyl peptidase 4 is a functional receptor for the emerging human coronavirus-EMC. Nature 495, 251–254.
Rana, S., Claas, C., Kretz, C.C., Nazarenko, I., Zoeller, M., 2011. Activation-induced internalization differs for the tetraspanins CD9 and Tspan8: impact on tumor cell motility. Int. J. Biochem. Cell Biol. 43, 106–119.
Rapaport, D., Ovadia, M., Shai, Y., 1995. A synthetic peptide corresponding to a conserved heptad repeat domain is a potent inhibitor of Sendai virus-cell fusion: an emerging similarity with functional domains of other viruses. EMBO J. 14, 5524–5531.
Reeves, J.D., Gallo, S.A., Ahmad, N., Miamidian, J.L., Harvey, P.E., Sharron, M., Pohlmann, S., Sfakianos, J.N., Derdeyn, C.A., Blumenthal, R., Hunter, E., Doms, R.W., 2002. Sensitivity of HIV-1 to entry inhibitors correlates with envelope/coreceptor affinity, receptor density, and fusion kinetics. Proc. Natl. Acad. Sci. Usa. 99, 16249–16254.
Schumann, J., Leichtle, A., Thiery, J., Fuhrmann, H., 2011. Fatty acid and peptide profiles in plasma membrane and membrane rafts of PUFA supplemented

RAW264.7 macrophages. PLoS One 6, e24066.
Scobey, T., Yount, B.L., Sims, A.C., Donaldson, E.F., Agnihothram, S.S., Menachery, V.D., Graham, R.L., Swanstrom, J., Bove, P.F., Kim, J.D., Grego, S., Randell, S.H., Baric, R.S., 2013. Reverse genetics with a full-length infectious cDNA of the Middle East respiratory syndrome coronavirus. Proc. Natl. Acad. Sci. USA 110, 16157–16162.
Shah, P.P., Wang, T., Kaletsky, R.L., Myers, M.C., Purvis, J.E., Jing, H., Huryn, D.M., Greenbaum, D.C., Smith, A.B., 3rd, Bates, P., Diamond, S.L., 2010. A small-molecule oxocarbazate inhibitor of human cathepsin L blocks severe acute respiratory syndrome and ebola pseudotype virus infection into human embryonic kidney 293T cells. Mol. Pharmacol. 78, 319–324.
Shen, B.Q., Finkbeiner, W.E., Wine, J.J., Mrsny, R.J., Widdicombe, J.H., 1994. Calu-3: a human airway epithelial cell line that shows cAMP-dependent Cl- secretion. Am. J. Physiol. 266, L493–L501.
Shen, X., Zhang, X., Liu, S., 2013. Novel hemagglutinin-based influenza virus inhibitors. J. Thorac. Dis. 5 (Suppl 2), S149–S159.
Shirato, K., Kanou, K., Kawase, M., Matsuyama, S., 2016. Clinical Isolates of Human Coronavirus 229E Bypass the Endosome for Cell Entry. J. Virol..
Shirato, K., Kawase, M., Matsuyama, S., 2013. Middle East respiratory syndrome coronavirus infection mediated by the transmembrane serine protease TMPRSS2. J. Virol. 87, 12552–12561.
Shulla, A., Gallagher, T., 2009. Role of spike protein endodomains in regulating coronavirus entry. J. Biol. Chem. 284, 32725–32734.
Shulla, A., Heald-Sargent, T., Subramanya, G., Zhao, J., Perlman, S., Gallagher, T., 2011. A transmembrane serine protease is linked to the severe acute respiratory syndrome coronavirus receptor and activates virus entry. J. Virol. 85, 873–882.
Simmons, G., Gosalia, D.N., Rennekamp, A.J., Reeves, J.D., Diamond, S.L., Bates, P., 2005. Inhibitors of cathepsin L prevent severe acute respiratory syndrome coronavirus entry. Proc. Natl. Acad. Sci. USA 102, 11876–11881.
Simmons, G., Zmora, P., Gierer, S., Heurich, A., Pohlmann, S., 2013. Proteolytic activation of the SARS-coronavirus spike protein: cutting enzymes at the cutting edge of antiviral research. Antivir. Res. 100, 605–614.
Thorp, E.B., Gallagher, T.M., 2004. Requirements for CEACAMs and cholesterol during murine coronavirus cell entry. J. Virol. 78, 2682–2692.
Ujike, M., Nishikawa, H., Otaka, A., Yamamoto, N., Yamamoto, N., Matsuoka, M., Kodama, E., Fujii, N., Taguchi, F., 2008. Heptad repeat-derived peptides block protease-mediated direct entry from the cell surface of severe acute respiratory syndrome coronavirus but not entry via the endosomal pathway. J. Virol. 82, 588–592.
van Boheemen, S., de Graaf, M., Lauber, C., Bestebroer, T.M., Raj, V.S., Zaki, A.M., Osterhaus, A.D., Haagmans, B.L., Gorbalenya, A.E., Snijder, E.J., Fouchier, R.A., 2012. Genomic characterization of a newly discovered coronavirus associated with acute respiratory distress syndrome in humans. mBio, 3.
Walls, A.C., Tortorici, M.A., Bosch, B.J., Frenz, B., Rottier, P.J., DiMaio, F., Rey, F.A., Veesler, D., 2016a. Cryo-electron microscopy structure of a coronavirus spike glycoprotein trimer. Nature 531, 114–117.
Walls, A.C., Tortorici, M.A., Frenz, B., Snijder, J., Li, W., Rey, F.A., DiMaio, F., Bosch, B.J., Veesler, D., 2016b. Glycan shield and epitope masking of a coronavirus spike protein observed by cryo-electron microscopy. Nat. Struct. Mol. Biol. 23, 899–905.
Weiss, S.R., Leibowitz, J.L., 2011. Coronavirus pathogenesis. Adv. Virus Res. 81, 85–164.
Weiss, S.R., Navas-Martin, S., 2005. Coronavirus pathogenesis and the emerging pathogen severe acute respiratory syndrome coronavirus. Microbiol. Mol. Biol. Rev. 69, 635–664.
Wild, C.T., Shugars, D.C., Greenwell, T.K., McDanal, C.B., Matthews, T.J., 1994. Peptides corresponding to a predictive alpha-helical domain of human immunodeficiency virus type 1 gp41 are potent inhibitors of virus infection. Proc. Natl. Acad. Sci. USA 91, 9770–9774.
Williams, R.K., Jiang, G.S., Holmes, K.V., 1991. Receptor for mouse hepatitis virus is a member of the carcinoembryonic antigen family of glycoproteins. Proc. Natl. Acad. Sci. USA 88, 5533–5536.
Xu, R., Wilson, I.A., 2011. Structural characterization of an early fusion intermediate of influenza virus hemagglutinin. J. Virol. 85, 5172–5182.
Xu, Y., Liu, Y., Lou, Z., Qin, L., Li, X., Bai, Z., Pang, H., Tien, P., Gao, G.F., Rao, Z., 2004a. Structural basis for coronavirus-mediated membrane fusion. Crystal structure of mouse hepatitis virus spike protein fusion core. J. Biol. Chem. 279, 30514–30522.
Xu, Y., Lou, Z., Liu, Y., Pang, H., Tien, P., Gao, G.F., Rao, Z., 2004b. Crystal structure of severe acute respiratory syndrome coronavirus spike protein fusion core. J. Biol. Chem. 279, 49414–49419.
Xu, Y., Zhu, J., Liu, Y., Lou, Z., Yuan, F., Liu, Y., Cole, D.K., Ni, L., Su, N., Qin, L., Li, X., Bai, Z., Bell, J.I., Pang, H., Tien, P., Gao, G.F., Rao, Z., 2004c. Characterization of the heptad repeat regions, HR1 and HR2, and design of a fusion core structure model of the spike protein from severe acute respiratory syndrome (SARS) coronavirus. Biochemistry 43, 14064–14071.
Yeager, C.L., Ashmun, R.A., Williams, R.K., Cardellichio, C.B., Shapiro, L.H., Look, A.T., Holmes, K.V., 1992. Human aminopeptidase N is a receptor for human coronavirus 229E. Nature 357, 420–422.
Young, J.K., Hicks, R.P., Wright, G.E., Morrison, T.G., 1997. Analysis of a peptide inhibitor of paramyxovirus (NDV) fusion using biological assays, NMR, and molecular modeling. Virology 238, 291–304.
Yuan, Y., Cao, D., Zhang, Y., Ma, J., Qi, J., Wang, Q., Lu, G., Wu, Y., Yan, J., Shi, Y., Zhang, X., Gao, G.F., 2017. Cryo-EM structures of MERS-CoV and SARS-CoV spike glycoproteins reveal the dynamic receptor binding domains. Nat. Commun. 8, 15092 .
Zelus, B.D., Schickli, J.H., Blau, D.M., Weiss, S.R., Holmes, K.V., 2003. Conformational changes in the spike glycoprotein of murine coronavirus are induced at 37 degrees C either by soluble murine CEACAM1 receptors or by pH 8. J. Virol. 77, 830–840.
Zhou, Y., Vedantham, P., Lu, K., Agudelo, J., Carrion, R., Jr, Nunneley, J.W., Barnard, D., Pohlmann, S., McKerrow, J.H., Renslo, A.R., Simmons, G., 2015. Protease inhibitors targeting coronavirus and filovirus entry. Antivir. Res. 116, 76–84.